The effect of resonance-assisted hydrogen bond on the second-order nonlinear optical properties of pyridine hydrazone photoswitches: a quantum chemistry investigation

Douniazed Hannachi, Noureddine Khelfaoui, Meriem Zaidi, Diha Yahiaoui, Salima Lakehal, Christophe Morell, Henry Chermette

ARTICLE

Received 00th January 20xx,

Accepted 00th January 20xx

DOI: 10.1039/x0xx00000x

The Effect of Resonance-Assisted Hydrogen Bond on the Second-Order Nonlinear Optical properties of Pyridine Hydrazone Photoswitches: A Quantum Chemistry Investigation

Douniazed Hannachi*[a, b], Noureddine Khelfaoui[a], Meriem Zaidi[a,c], Diha Yahiaoui[a], Salima Lakehal[d], Christophe Morell[e], Henry Chermette*[e]

The incidence of hydrogen bonds on NLO properties was not considered as essential, in particular in Pyridine Hydrazone systems, yet we show in the present work that a control of these photoswitches depends on the strength of hydrogen bonds. In this study, we investigate a selection of 18 E/Z Pyridine Hydrazone photoswitch molecules to explore the impact of resonance –assisted hydrogen bond (RAHB) on the NLO properties in the E/Z isomers. Using quantum calculations at the ωB97XD/6-311+g(d) level of theory, we determine various electronic parameters, reactivity descriptors, bond length alternation (BLA) values, Nuclear Independent Chemical Shift (NICS) aromaticity indices, QTAIM topology, energy of hydrogen bond (E_{HB}), RAHB as well as linear and nonlinear optical properties for these molecules. The agreement between the quantum calculations and experimental spectra is illustrated through TD-DFT calculations, showing small deviations. Contrary to conventional expectations, our findings demonstrated that the delocalization strength of the electrons and NLO properties of the Z isomers is significantly enhanced by the presence of a resonance –assisted hydrogen bond. The Z-isomer exhibited a lower excited state energy, weaker energy gap, smaller BLA value, larger dipole moment variations for the first excited state, higher $\Phi_{E\to Z}$, and electron delocalization at the quasi -cycle closed (RAHB) compared to the E-isomer. Furthermore, we find that the hyperpolarizability value of the title photoswitches increases as the wavelength of the incident light decreases, i.e., β(695)>β(1064)>β(1340)>β(∞) and the dispersion has less effect at λ=1064 and 1340 nm. Additionally, we observe a strong relation between the photoisomerization quantum yield ($\Phi_{E\rightleftarrows Z}$) and static hyperpolarizability (b) of the first and second isomer, where $\Phi_{E\rightleftarrows Z}$ is proportional to b of the second isomer and inversely proportional to b of first isomer. This inverse trend between static hyperpolarizability and photoisomerization quantum yields is attributed to the electron-withdrawing character of substituents on the Ar ring. Our research provides valuable insights into optimizing the 2nd-order NLO properties of Pyridine Hydrazone photoswitch molecules. Through understanding the influence of hydrogen bonding on delocalization strength of the electrons (RAHB) and the shape-dependent NLO performance, we gain the ability to design and synthesize novel photoswitch molecules with enhanced NLO characteristics.

Introduction

Molecular photoswitches are defined as chemical compounds that can reversibly be transformed from one isomer into another one with light irradiation. The two isomers differ from each other in various chemical and physical properties, such as geometrical structure, absorption spectra, oxidation/reduction potentials, magnetic properties, dielectric constant, and refractive index, and so forth.[1,2] This kind of molecules provides an invaluable tool for a large variety of applications such as in information storage and processing[3], photo-pharmacology, photo-actuators, remote-controllable reactions, controllable drug transport and release, etc.[4,5]

Nonlinear optics (NLO) is a branch of optics that deals with phenomena arising from light-induced changes in the optical properties of compounds (e.g., phase, frequency, amplitude, polarization, path, etc.). NLO compounds are materials that exhibit nonlinear optical responses, such as second-harmonic generation (SHG), Optical Kerr effect and third-harmonic generation (THG). These compounds have a wide range of applications in different fields such as optical communication, optical computing, optical memory and all-optical signal processing. [6–11] The photochromic compounds, like stilbenes, azobenzenes[12–14], diarylethenes[15], spiropyrans[16], fulgides[4,17] have excellent nonlinear optical responses (high hyperpolarizability). The combination between these two properties (photochromic and nonlinear optical) empowers generations of switchable second-order NLO materials. These classes of materials are called optical switches and have very high applications in optoelectronic and photonic technologies, including molecular-scale memory devices with multiple storage and non-destructive reading capacity[18]. It is important to note that the photoswitching of second-order NLO properties makes sense

[a.] *Laboratoire d'Électrochimie, d'Ingénierie Moléculaire et de Catalyse Redox (LEIMCR), Département d'Enseignement de Base en Technologie, Faculté de Technologie, Université Ferhat Abbas, Sétif-1, Algérie.*
[b.] *Département de Chimie, Faculté des Sciences, Université Ferhat Abbas, Setif-1, Algérie.*
[c.] *Laboratoire de Chimie, Ingénierie Moléculaire et Nanostructures (LCIMN), Université Ferhat Abbas Sétif 1, Sétif 19000, Algerie.*
[d.] *Institut des Science de la Terre et de l'Univers, Université de Batna-2, Algérie.*
[e.] *Université de Lyon, Université Claude Bernard Lyon 1, Institut des Sciences Analytiques, UMR CNRS 5280, 69622 Villeurbanne Cedex, France*
† Footnotes relating to the title and/or authors should appear here.
Electronic Supplementary Information (ESI) available: [details of any supplementary information available should be included here]. See DOI: 10.1039/x0xx00000x

only when the photoisomer compounds are thermally stable[19]. From the literature, the switching of NLO properties has been performed by specific procedures including protonation/deprotonation, oxidation/reduction, and photoisomerization.[20–24] In our work we used the photoisomerization to switch the NLO properties.

Recently, Mravec and collaborators[25–27] designed and synthesized an extended set of 13 pyridine/quinoline hydrazones photoswitches. This new class of hydrazone-based P-type photoswitches is switchable between two isomers Z and E (see Figure 1) and shows excellent thermal stability of both isomers. The operational wavelengths of the pyridine hydrazone structural motif shifted toward the visible region without accompanying loss of their high thermal stability and hydrazone 7 retains good thermal stability[25]. Furthermore, the quantum-chemical calculations at the ωB97XD/def2-TZVPP level revealed a three-step inversion-rotation reaction mechanism of the thermal E-to-Z isomer. For benzoylpyridine hydrazones 1-8, 10 and 16, the E-to-Z photoisomerization is more efficient compared to the Z-to-E process. From the work of Mravec et al.[25] we can note that these compounds could be used for short-lived and long-lived information storage[28] as well as these isomers could be utilized as photoswitch molecules.

In our work, we studied a series of 18 pyridine hydrazone photoswitches (Zi and Ei isomers, i= 1- 18, see Figure 1) which is divided in two subgroups namely, one group of ten Zi and Ei isomers (where i=1-8, 10 and 16) synthesized by Mravec et al.[25] and another one we designed and consisting in eight compounds (i=9, 11-15 and 17-18 of Ei and Zi isomers) to investigate the substitutional effect on the hydrazine and ketone parts on the structural, electronic, reactivity, optical properties and nonlinear responses. On ring 2, we chose two electron-withdrawing (EW) namely NO_2 and CN in order to study the effect of the EW character on electronic and optical properties. The main objective of this work is to show how the hydrogen bond can enhance the NLO properties of the pyridine hydrazones photoswitches and try to find a relation between photoisomerization direction ($E \rightleftarrows Z$) and hyperpolarizability.

The present paper is organized as follows: In Section 1, all computational details in the corresponding section and definitions are given; in Section 2 the quantum theory of atom-in-molecules (QTAIM) is analyzed; in Section 3 the bond length alternation (BLA) is presented; in Section 4 the Nuclear Independent Chemical Shift (NICS) aromaticity indices are evaluated; in Section 5 the Resonance assisted hydrogen bond; in Section 6 the global Reactivity descriptors are studied; in Section 7 the absorption spectra are discussed; and in Section 8 the static and dynamic NLO responses of E and Z isomers are calculated; the paper ends with some concluding remarks.

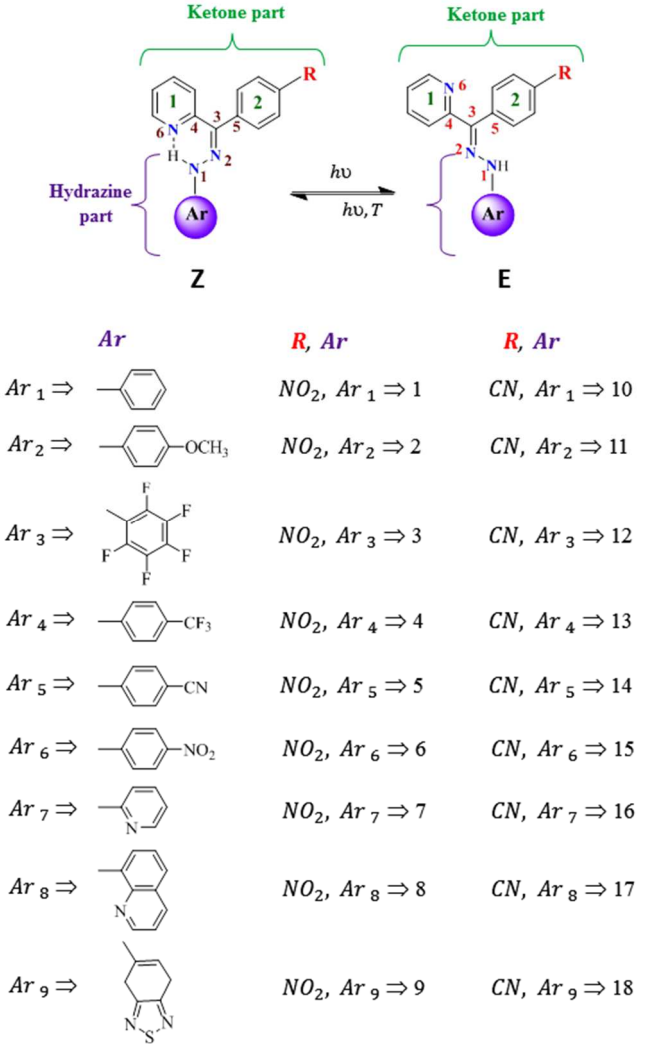

Figure 1 Chemical structures of the pyridine hydrazones photoswitches (from the Ref.25 for i=1-8, 10 and 16)

Computational details

The geometries of the E and Z isomers were fully optimized using the ωB97XD density functional[29,30] with 6-311+g(d) basis set[31,32]. The ωB97XD is a range-separated hybrid exchange-correlation functional that includes damped atom-atom dispersion corrections[29,33]. The quantum chemistry calculations were performed with Gaussian 09 program with the TIGHT SCF convergence and ultra-fine integration grid[34–36]. No symmetry constraints were applied and the local minima confirmed on potential energy surface by harmonic frequency calculations of the ground state for E and Z isomers at the same level. All the calculations were performed in the gas phase

Chemical reactivity descriptors such as chemical hardness (η), electronic chemical potential (μ) and electronegativity (χ) can be evaluated from the frontier orbital energies HOMO and LUMO (ε_H and ε_L, respectively) by the following equation [37]

$$\mu = \frac{1}{2}(\varepsilon_H + \varepsilon_L) = -\chi \qquad (1)$$

$$\eta = \varepsilon_L - \varepsilon_H \quad (2)$$

The chemical hardness (η) measures the stability of a molecule in terms of resistance to electron transfer and the chemical potential (μ) characterizes the escaping tendency of electrons from the equilibrium system. The global electrophilicity index (ω), introduced by Parr et al.[38], is calculated from the hardness and chemical potential:

$$\omega = \frac{\mu^2}{2\eta} \quad (3)$$

This index expresses the ability of a molecule to accept electrons from the environment.

Time-dependent density functional theory (TD-DFT) calculations were carried out at the same level of theory to evaluate absorption wavelengths (λ) and corresponding oscillator strengths (f_{osc}) of electronic transitions. For TD-DFT calculations, sixty excited states have been calculated.

Following the procedure proposed by LeBahers et al.[39] the excited states of interest were examined using charge-transfer indices (CT) including charge-transfer distance (d^{CT}), transferred charge (q^{CT}) and the variation in dipole moment between the ground and the excited states ($\Delta\mu_{0\to n} = q^{CT} \times d^{CT}$). In our work, the CT indices have been examined with MULTIWFN program[40].

The electron density difference maps (EDDM) corresponding to the crucial excited states can be exactly evaluated as follows:

$$\Delta\rho(r) = \rho_{ex}(r) - \rho_{GS}(r) \quad (4)$$

$\rho_{ex}(r)$ and $\rho_{GS}(r)$ defining as the electronic densities associated to the excited and ground states, respectively.

On the other hand, isotropic polarizability (α), polarizability density (ρ) and first hyperpolarizability (β_0) are calculated using analytical derivatives of the system energy (coupled-perturbed Kohn – Sham method)[41] at the ωB97XD /6-311+g(d) level of theory. These parameters are defined as[8,42]:

$$\alpha = \frac{1}{3}(\alpha_{xx} + \alpha_{yy} + \alpha_{zz}) \quad (5)$$

$$\rho = \frac{<\alpha>}{V} \quad (6)$$

$$<\beta> = \sqrt[2]{\beta_x^2 + \beta_y^2 + \beta_z^2} \quad (7)$$

In this work we also analyzed the second-harmonic generation ($\beta_{SHG}(-2\omega;\omega,\omega)$), electro-optical Pockels effect (β(-ω;ω,0)), Hyper-Rayleigh scattering responses (β_{HRS}) and depolarization ratios (DR) [8,43,44] at selected three frequencies (ω). Among these, two laser frequencies 0.0340 a.u (1340 nm) and 0.0428 a.u (1064 nm) are fed into these isomers. The frequency 0.0656 a.u (695 nm) has also been imposed on these isomers. At dynamic regime the components of β_i are represented as:

For the second harmonic generation:

$$\beta_i = \beta_{iii}(-2\omega;\ \omega,\omega) + \beta_{ijj}(-2\omega;\ \omega,\omega) + \beta_{ikk}(-2\omega;\ \omega,\omega) \quad (8)$$

In the case of electro-optical Pockels effect the β_i obtained by:

$$\beta_i = \beta_{iii}(-\omega;\ \omega,0) + \beta_{ijj}(-\omega;\ \omega,0) + \beta_{ikk}(-\omega;\ \omega,0) \quad (9)$$

The second-order NLO response β_{HRS} is given by[44]:

$$\langle\beta_{HRS}\rangle = \sqrt{\{\langle\beta_{ZZZ}^2\rangle + \langle\beta_{XZZ}^2\rangle\}} \quad (10)$$

Where $\langle\beta^2_{ZZZ}\rangle$ and $\langle\beta^2_{XZZ}\rangle$ are orientational averages of the β tensor without assuming Kleinman's conditions. furthermore, β is typically decomposed into the sum of dipolar (J=1) and octupolar (J=3) tensorial components[45]:

$$\langle\beta_{ZZZ}^2\rangle = \frac{9}{45}\left|\beta_{J=1}\right|^2 + \frac{6}{105}\left|\beta_{J=3}\right|^2 \quad (11)$$

$$\langle\beta_{XZZ}^2\rangle = \frac{1}{45}\left|\beta_{J=1}\right|^2 + \frac{4}{105}\left|\beta_{J=3}\right|^2 \quad (12)$$

The depolarization ratios (DR) provide information upon the shape of the geometry of the chromophore, the part of the compound responsible for the NLO response (for an ideal one-dimensional system DR = 5, for an octupolar molecule DR = 1.5)

$$DR = \frac{\langle\beta_{ZZZ}^2\rangle}{\langle\beta_{XZZ}^2\rangle} \quad (13)$$

Results and Discussion

Topological study

The intramolecular H-bond is one of the most prominent features which could influence the stability of compounds[46]. In this paper, we use the quantum theory of atom-in-molecules (QTAIM) to examine this bond[47,48]. In this theory, the critical points (in ring (RCP) or bond (BCP)) are the positions where the gradient is null and which can be classified according to the electron density (ρ) and its Laplacian ($\nabla^2(\rho)$), total electron energy density (H), kinetic electron energy density (G) and potential electron energy density (V).[47,49] The QTAIM calculations were carried out for Z-isomers using the Amsterdam Density Functional (ADF18) program developed by Baerends *et al.*[50,51] and the results of the calculation are gathered in Table S1. Figure 2 depicts the molecular graphs corresponding to Z6 isomer where the red circle indicates the ring critical point (RCPs) and the green circle indicates the bond critical point (BCPs).

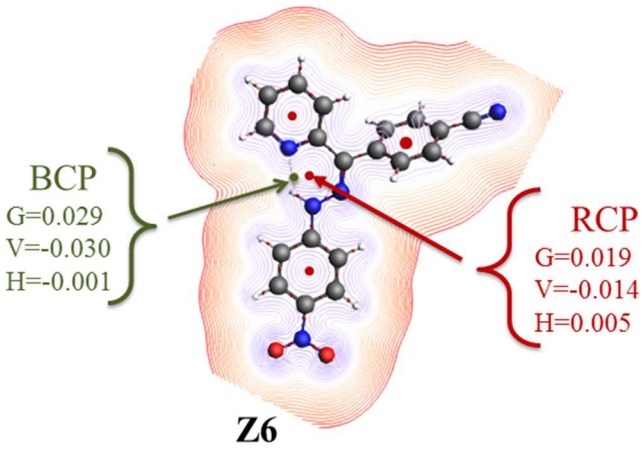

Figure 2 Molecular topology of Z6-isomer

In all of the Z-isomers, ring critical point (RCP: N1-N2-C3-C4-N6…H) and hydrogen bonds between the ketone and hydrazine moiety are observed (see Table S1 and Figure 2). It is interesting to note that the formation of this RCP resulted from the cyclic nature of electron current and also confirms the existence of hydrogen bonding (N1-H…N6).

The QTAIM analysis shows that the critical point at the hydrogen bond N1-H…N6 (BCP) has electronic density ranges from 0.012 to 0.015 a.u., while the Laplacian of the electron densities is from 0.96-0.100 a.u., G= 0.019, V= -0.014 and H= 0.005 (with the exception of the isomers substituted with Ar7 and Ar8, where the H value amounts from -0.0005 to -0.0003 a.u.). Whereas for the ring critical points (RCP: N1-N2-C3-C4-N6…H) the values electronic

density ranges from 0.031-0.035 and its Laplacian is from 0.103 to 0.109, the value of G, V and H are 0.028, -0.027 to -0.030 and 0.05 a.u., respectively. From this value, we note that there is no effect of the substitutions (Ar moiety and EW groups (CN, NO_2) at the ring 2) on H-bond and RCP (see Table S1). On the other hand, H-bond exhibits positive values of $\nabla^2(\rho_{BCP})$ and negative values of H_{BCP} are typical of intermediate hydrogen bonds. Furthermore, in the RCP we observe an increase of the kinetic energy (G) over the potential energy |V| this means that the electrons are moving faster in ring N1-N2-C3-C4-N6…H or in other words the electrons are less localized. In the case of BCP H-bond (H…N6) we note that $G \leq |V|$, indicating that in this in region of Z-isomers the electrons are localized[52].

On the other hand, the BLA is a structural parameter, defined as the average difference between the lengths of a single bond and the adjacent multiple bonds in a π-delocalized isomer. For the title isomers we calculated the BLAs (*BLA₁* and *BLA₂*, see atom numbering in Figure 1) and gathered in Table 1.

Table 1 Bond length alternation (BLA_1 and BLA_2, Å) for the Ei and Zi (i=1 to 18) compounds

Ei	BLA_1	BLA_2	Zi	BLA_1	BLA_2	Ei	BLA_1	BLA_2	Zi	BLA_1	BLA_2
E1	0.120	0.126	**Z1**	0.104	0.107	**E10**	0.120	0.126	**Z10**	0.104	0.108
E2	0.119	0.125	**Z2**	0.099	0.103	**E11**	0.119	0.125	**Z11**	0.100	0.104
E3	0.140	0.143	**Z3**	0.125	0.125	**E12**	0.141	0.144	**Z12**	0.113	0.114
E4	0.125	0.130	**Z4**	0.111	0.114	**E13**	0.125	0.130	**Z13**	0.111	0.114
E5	0.126	0.132	**Z5**	0.113	0.116	**E14**	0.127	0.132	**Z14**	0.114	0.117
E6	0.128	0.132	**Z6**	0.115	0.118	**E15**	0.128	0.133	**Z15**	0.116	0.118
E7	0.124	0.128	**Z7**	0.110	0.113	**E16**	0.123	0.128	**Z16**	0.111	0.113
E8	0.121	0.126	**Z8**	0.108	0.110	**E17**	0.122	0.126	**Z17**	0.110	0.112
E9	0.125	0.130	**Z9**	0.111	0.113	**E18**	0.125	0.131	**Z18**	0.112	0.114

$BLA_1 = 1/2\ (d_{1-2} + d_{3-4} - 2d_{2-3})$

$BLA_2 = 1/2\ (d_{1-2} + d_{3-5} - 2d_{2-3})$

The DFT calculation shows that in the whole set of isomers (Z and E) the BLA_1 is smaller than the BLA_2, which may be ascribed to the donation effect of pyridine ring (ring 1, see Figure 1). When comparing E1-E9 isomers to E10-E18, it is found that the BLA_1 and BLA_2 values of Ei–isomers substituted by NO_2 group are similar to that of the Ei-isomers substituted by CN group. For example BLA_1= 0.128 and BLA_2= 0.132 Å for E6 and E16. The same results we observed for the Z–isomers, with the exception of Z3 and Z12 compounds where the values are different (BLA_1(Z3) = 0.125 ≠ BLA_1(Z12) = 0.113 and BLA_2(Z3) = 0.125 ≠ BLA_2(Z12) = 0.114. From these results we can conclude that the substitution of a NO_2 by a CN group in R position does not introduce significant changes in the bond length alternation BLA_1 and BLA_2 along the conjugated linker which connects the Ar and ketone parts. On the other hand, we observe that the BLA_{1-2} values of the Z1-Z18 isomers are smaller than that of the corresponding E1-E18 isomers. This suggests that the π-conjugation of the Z–isomers is stronger than that of the corresponding E–isomers, this is certainly related to the existence of the hydrogen bond N1-H...N6 (stronger electrostatic effects in the Z–isomers). In addition, the smallest BLA_{1-2} values are obtained when Ar is C_6H_4-p-OCH_3 (Ar_2) group (isomers Z2, Z11 and E2, E11) whereas the largest values are obtained for Ar_3 = C_6F_6 (E3, E12, Z3 and Z12 isomers). Thus, the effect of the nature of the Ar group is stronger for the BLA_1 and BLA_2 values than the nature of the R substituent (NO_2 and CN). Generally, the BLA_{1-2} values of Z1-Z9, Z10-18, E1-E9 and E10-18 isomers increase following the order: Ar_2 < Ar_1 < Ar_8 < Ar_7 < Ar_9 < Ar_4 <Ar_5 < Ar_6 < Ar_3. From this result we can note that the BLA_{1-2} values increases with increase in the EW character of the substituents on the Ar-ring.

The calculated hydrogen bond angle and dihedral angle between the hydrazine part and rings 1 and 2 are listed in table S2 (Supporting Information). Regardless of the nature of the R substituent, we observed that the E to Z isomerization results in a decrease in the dihedral angle φ_1 by approximately 27°, while φ_2 deviates by 74°. On the other hand, for the Z isomers, it is found that the dihedral angle (φ_1) measured between ring 1 and the hydrazine part is approximately 19°, which is smaller compared to the dihedral angle between ring 2 and the hydrazine part (φ_2 = 44°). This decrease in angle (φ_1) enhances the π-electron conjugation between ring 1 and the hydrazine part more than between ring 2 and the hydrazine part. Additionally, the hydrogen bonds presence leads to reduced dihedral angles between the Ar-linker-ring 2 in the Z-isomer. This observation is reinforced by the slightly lower bond length alternation (BLA2) values in the Z-isomer compared to the E-isomer.

On the other hand, for the Z isomers, the N1-H...N6 hydrogen bond angle (φ_3) has been observed to be 130°. However, an exception is noted in Z7, Z8, Z16, and Z17, where the angle φ_3 is measured at 127° (table S2). Notably, this angle aligns well with the IUPAC recommendations, which suggest that hydrogen bond angles should preferably be above 110°.[53]

Aromaticity

The local aromaticity, non-aromaticity as well as anti-aromaticity in the title compounds is assessed by Nuclear Independent Chemical Shift (NICS) calculations which was introduced by von Ragué Schleyer et al. [54,55] The NICS was calculated at the ring center or cages and described as the negative value of the isotropic shielding constant.[56] Noted that the strongly negative NICS values (i.e. magnetically shielded) denote the presence of induced diatropic ring currents and "aromaticity", whereas the positive values (i.e. deshielded) at chosen point indicate paratropic ring current and "anti-aromaticity".[57] In this work we used $NICS_{ZZ}(1)$ index, which is calculated in 1Å above the center of the ring under consideration. Results of $NICS_{ZZ}(1)$ calculation for all isomers considered are listed in Table 2.

For the both isomers, the quantum calculation shows that the $NICS_{zz}(1)$ index is more negative in rings 2 than in the ring 1. The aromaticity in ring 2 substituted with NO_2 group is notably smaller than that substituted with CN group (with the exception of isomers E2, E5 and E8). At the same time, localization of NO_2 group at ring 2 results in increases of the anti-aromaticity of quasi -cycle closed, with exception for the 3 and 8 compounds. Altogether, it leads to lower stability of these isomers (Z1 to Z9) in comparison with the isomers Z10 to Z18 (CN group at the ring 2). On the other hand, the $NICS_{zz}(1)$ results obtained for Ar-ring (ring 3) indicate that this ring is aromatic and less stable than the ring 2, with the exception of the compounds 3 and 12, where Ar3 exhibits a high aromaticity diatropicity and stability. The order of $NICS_{zz}(1)$ index of Ar-ring is Ar3> Ar2> Ar1> Ar8> Ar4> Ar5> Ar7> Ar6> Ar9.

$NICS_{zz}(1)$ indexes for Z isomers reveal a reduction in aromatic behavior in rings 2 and Ar, whereas ring 1 shows an increase in

aromatic character in comparison with corresponding E isomers (Table 2). These variations in aromaticity between Z and E isomers can be attributed to the RAHB effect and pronounced anti-aromatic behavior in quasi -cycle closed in Z isomers. In general, we can conclude that the Z–isomer displays a smaller BLA value as well as larger aromatic character (ring 1) than that of the corresponding E–isomer.

Mravec et al. found that the benzoylpyridine hydrazones 1−8, 10 and 16, the E→Z photoisomerizatione is more efficient compared to the Z→E process.[25] We can attribute these results to the Z-isomer shape, which features an antiaromatic ring (quasi-cycle closed) surrounded by three aromatic rings (1, 2 and Ar ring).

Table 2 NICSzz aromaticity index

		$NICS_{zz}$			$NICS_{zz}$			$NICS_{zz}$			$NICS_{zz}$
E1	1	-8.089	**Z1**	1	-9.396	**E10**	1	-8.120	**Z10**	1	-9.385
	2	-12.941		2	-10.109		2	-13.197		2	-10.709
	3	-9.693		3	-9.387		3	-9.520		3	-9.405
				QCC	27.197					QCC	27.227
E2	1	-8.160	**Z2**	1	-9.370	**E11**	1	-7.941	**Z11**	1	-9.275
	2	-13.098		2	-9.958		2	-12.942		2	-10.621
	3	-10.122		3	-8.630		3	-10.031		3	-8.600
				QCC	26.980					QCC	27.051
E3	1	-8.796	**Z3**	1	-10.370	**E12**	1	-8.802	**Z12**	1	-10.318
	2	-13.019		2	-10.217		2	-13.119		2	-10.527
	3	-15.667		3	-15.404		3	-15.846		3	-15.612
				QCC	27.127					QCC	27.027
E4	1	-8.406	**Z4**	1	-9.924	**E13**	1	-8.287	**Z13**	1	-9.827
	2	-13.065		2	-10.738		2	-13.843		2	-11.812
	3	-7.719		3	-7.657		3	-7.644		3	-7.566
				QCC	27.357					QCC	27.406
E5	1	-8.826	**Z5**	1	-10.058	**E14**	1	-8.482	**Z14**	1	-9.995
	2	-13.338		2	-10.960		2	-13.260		2	-11.221
	3	-7.479		3	-7.216		3	-7.364		3	-7.265
				QCC	27.323					QCC	27.358
E6	1	-8.798	**Z6**	1	-10.147	**E15**	1	-8.491	**Z15**	1	-9.987
	2	-13.193		2	-10.989		2	-13.217		2	-11.256
	3	-6.483		3	-6.090		3	-6.348		3	-6.267
				QCC	27.459					QCC	27.630
E7	1	-8.362	**Z7**	1	-9.875	**E16**	1	-8.324	**Z16**	1	-9.856
	2	-12.849		2	-10.303		2	-13.101		2	-10.786
	3	-6.512		3	-6.562		3	-6.335		3	-6.678
				QCC	26.969					QCC	27.113
E8	1	-7.902	**Z8**	1	-9.346	**E17**	1	-8.237	**Z17**	1	-9.230
	2	-12.916		2	-9.793		2	-12.893		2	-10.319
	3	-8.522		3	-8.596		3	-8.409		3	-8.293
		-8.961		QCC	28.264			-8.984		QCC	28.214
	1′			1′	-9.009		1′			1′	-8.838
E9	1	-8.864	**Z9**	1	-9.902	**E18**	1	-8.388	**Z18**	1	-9.879
	2	-13.341		2	-10.205		2	-13.466		2	-10.747
	3	-0.342		3	-0.216		3	-0.288		3	-0.0602
		-13.128		QCC	27.615			-13.171		QCC	27.736
	1′			1′	-14.047		1′			1′	-12.639

Resonance assisted hydrogen bond

Table 3 Summarizes of the δ_{N_1H} chemical shifts (ppm), σ_{N_1H} stretching frequency (cm^{-1}) and the distance r_{N_1-H} (Å) for Ei and Zi (i=1 to 18) isomers. The energy of HB ($E_{HB}(V)$ kcal/mol), and distance ($r_{H\ldots N_6}$, $r_{N_1-N_6}$Å) for each Z isomers are also given

	δ_{N_1H}	σ_{N_1H}	r_{N_1-H}		δ_{N_1H}	σ_{N_1H}	r_{N_1-H}	$r_{H\ldots N_6}$	$r_{N_1-N_6}$	$E_{HB}(V)$
E1	6.32	3576.90	1.012	**Z1**	12.26	3500.52	1.016	1.921	2.695	4.59
E2	6.04	3578.16	1.012	**Z2**	12.21	3489.31	1.017	1.919	2.691	4.59
E3	5.62	3565.79	1.013	**Z3**	11.70	3465.57	1.018	1.913	2.682	4.59
E4	6.25	3579.79	1.012	**Z4**	12.25	3496.47	1.017	1.916	2.693	4.59
E5	6.11	3576.89	1.012	**Z5**	12.38	3500.48	1.017	1.913	2.690	4.76
E6	6.28	3578.79	1.012	**Z6**	12.43	3474.69	1.017	1.907	2.688	4.76
E7	7.00	3571.91	1.013	**Z7**	12.32	3506.80	1.017	1.956	2.700	4.06
E8	8.76	3555.43	1.014	**Z8**	13.58	3481.68	1.018	1.946	2.691	4.24
E9	5.98	3581.15	1.012	**Z9**	12.14	3486.62	1.016	1.915	2.692	4.59
E10	6.13	3577.43	1.012	**Z10**	12.36	3492.43	1.016	1.914	2.689	4.76
E11	6.22	3576.14	1.012	**Z11**	12.18	3489.44	1.016	1.917	2.692	4.59
E12	5.60	3562.77	1.014	**Z12**	11.49	3478.79	1.017	1.923	2.687	4.59
E13	6.28	3579.79	1.012	**Z13**	12.19	3496.47	1.017	1.916	2.693	4.76
E14	6.13	3576.36	1.012	**Z14**	12.28	3491.46	1.017	1.913	2.691	4.76
E15	6.23	3576.04	1.012	**Z15**	12.37	3496.83	1.017	1.909	2.688	4.76
E16	6.87	3576.35	1.013	**Z16**	12.40	3507.92	1.017	1.949	2.695	4.24
E17	8.78	3553.10	1.014	**Z17**	13.51	3482.99	1.018	1.949	2.693	4.24
E18	5.95	3580.07	1.012	**Z18**	12.20	3491.47	1.016	1.917	2.691	4.59

Based on the analyses of the data presented in Table 3, the E-isomers exhibit a chemical shift of the bridging hydrogen at the range of $\delta_{N_1H,E} = 5.6 - 8.8$ ppm, and the $N_1 - H$ stretching frequency at the range of $\sigma_{N_1H,E} = 3553 - 3581$ cm^{-1}. On the other hand, the Z isomers display significantly higher δ_{N_1H} ($\delta_{N_1H,Z} = 11.7 - 13.5$ ppm) and lower σ_{N_1H} values ($\sigma_{N_1H,Z} = 3465 - 3508\ cm^{-1}$) compared to the corresponding E-isomer. The observed variations in Z isomers are a result of the presence of intramolecular N1-H…N6 hydrogen bonding, leading to the formation of a quasi-ring structure N1-N2-C3-C4-N6…H (the distance N1-N6 and H…N6 is ~2.691 and 1.922 Å). According to the literature and our calculations, this quasi-ring structure is almost planar[58–65] (see Table S2) and distinguished by short N1-N6 distances and longer H-N1 bonds ($r_{HN_1,Z} \approx 1.018$ Å and $r_{HN_1,E} \approx 1.012$ Å). Furthermore, the analysis using QTAIM indicates a delocalization of electrons within the quasi-cycle closed (RCP). Additionally, we observed lower $\delta_{N_1H,Z}$ frequencies and downfield shift of the $\delta_{N_1H,Z}$. These findings strongly support the resonance-assisted hydrogen bond model (RAHB) proposed by Gilli et al.[66–68]

and we can conclude that this quasi -cycle closed (QCC) created a RAHB phenomenon.

We note that in the closed quasi-cycle of the Z isomer, the enhancement of conjugation results from the effective charge transfer occurring between the π-donor amine nitrogen to the pyridine nitrogen through the C=N double bond. This charge transfer is notably more efficient compared to a similar transfer in the open quasi-cycle of the E isomer, where it is attributed to the formation of a RAHB system.

Numerous methods have emerged over time to estimate the energy of hydrogen bonds. Among these, the widely employed approach for estimating E_{HB} involves utilizing the relation established by Espinosa et al. According to their work, the potential electron energy density (V) at the BCP is directly proportional to the energy of the hydrogen bond (E_{HB}), with an angular coefficient of 0.5. [69] Despite its popularity, Espinosa's equation tends to yield a significantly overestimated energy of HB. [70,71] More recently, Afonin et al. introduced a novel linear relationship between the calculated (V) and the energy (E) of hydrogen bonds.[72] They achieved this by utilizing empirical 1H NMR data and represented it as "eqn-14".

$$E_{HB}(V) = 0.277 \times |V| - 0.45 \qquad (14)$$

In order to assess the strength of the hydrogen bond, we employed equation (14) and presented the corresponding calculation results in Table 3. The analysis demonstrates that the hydrogen bond energy in the Z isomers varies between 4.1 and 4.8 kcal/mol, placing them within the category of medium-strength hydrogen bonds.[72] It is worth mentioning that the relatively weak energy of the $E_{HB}(V)$ does not have a significant impact on the optical properties of photoswitches.

Reactivity

The values of global reactivity descriptors chemical potential (μ), hardness (η) and electrophilicity index (ω) calculated for each Ei and Zi isomers (i=1 to 18) are collected and presented in Table 4 and Figure 3.

Table 4 Chemical potential (μ, eV), chemical hardness (η, eV) and electrophilicity index (ω, eV) of the Ei and Zi (i=1 to 18) compounds

	μ	η	ω		μ	η	ω
E1	-4.277	6.617	1.382	**Z1**	-4.163	6.574	1.318
E2	-4.230	6.536	1.369	**Z2**	-3.969	6.304	1.249
E3	-4.736	7.270	1.542	**Z3**	-4.596	7.057	1.497
E4	-4.550	6.863	1.509	**Z4**	-4.442	6.792	1.452
E5	-4.602	6.868	1.542	**Z5**	-4.511	6.768	1.503
E6	-4.706	6.968	1.589	**Z6**	-4.630	6.822	1.571
E7	-4.380	6.923	1.385	**Z7**	-4.314	6.764	1.376
E8	-4.116	6.549	1.293	**Z8**	-4.075	6.414	1.294
E9	-4.460	6.709	1.482	**Z9**	-4.400	6.548	1.478
E10	-3.881	7.335	1.027	**Z10**	-3.903	6.991	1.089
E11	-3.850	7.214	1.027	**Z11**	-3.692	6.758	1.009
E12	-4.410	7.888	1.233	**Z12**	-4.384	7.382	1.302
E13	-4.201	7.495	1.177	**Z13**	-4.233	7.111	1.269
E14	-4.292	7.421	1.241	**Z14**	-4.330	7.027	1.334
E15	-4.534	7.248	1.418	**Z15**	-4.509	6.966	1.459
E16	-4.031	7.544	1.077	**Z16**	-4.046	7.186	1.139
E17	-3.856	7.004	1.061	**Z17**	-3.854	6.757	1.099
E18	-4.340	6.892	1.366	**Z18**	-4.292	6.674	1.380

From these results we can see that the E-isomers show the largest values of the chemical hardness which signifies a greater stability and lower reactivity, whereas the smallest value of hardness are observed for the corresponding Z-isomers, this observation is in line with the experimental results of Mravec et al.[25]. The overall increasing order of hardness in the studied compounds is as follows: E2 <E8 <E1 <E9 <E4 <E5 <E18 <E7 <E6 <E17 <E11 <E15 <E3 <E10 <E14 <E13 <E16 <E12. The same order is observed for corresponding Z-isomers see Figure 3.

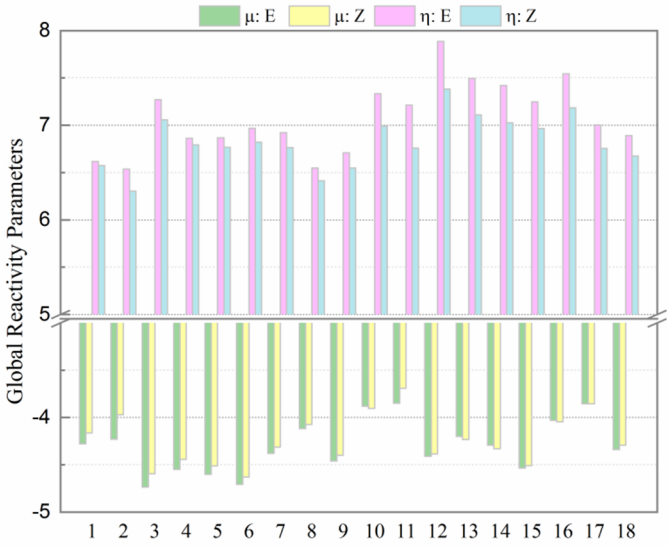

Figure 3 Global reactivity indices of Ei and Zi (i=1 to 18) isomers

On the other hand, the potential chemistry of Z-isomers is larger than that of the corresponding E-isomer. These results indicate that the trend of the electrons to leave the equilibrium systems increases from Z to E isomers. In other words, the rise of the μ values indicates that the isomers with RAHB system have the biggest tendency to donate electrons.

The chemical potential values of E/Z isomers increase in the following order:

E3<E6<E5<E4<E15<E9<E12<E7<E18<E14<E1<E2<E13<E8<E16<E10<E17<E11

According to the global electrophilicity scale[56,73] the Ei and Zi isomers where i=1 to 9 (with electron-withdrawing NO_2) and i= 12, 14-15, 18 and Z13 can be classified as strong electrophiles (1.23 to 1.58 eV). Besides, the Zi and Ei isomers of i= 10, 11, 16-17 and E13 (CN substituent) display a moderate electrophilicity power (1.00 to 1.17 eV)

Linear optical properties

The calculated excited state transition energies (ΔE), wavelength (λ), oscillator strengths (*f*), charge transfer (q^{CT}, |e|), charge

transfer distance (d^{CT}, Å), dipole moment variation ($\Delta\mu$, D) and major molecular orbital transitions of isomers are summarized in Table 5 and Table S3. Furthermore, the shapes of the MOs of specific excitation and EDDM for all isomers are provided in the Supporting Information (Figure S1 and S2)

Theoretically, the electron transition energy is a decisive property of optical absorption because it is closely related to the position of the maximum absorption peak (λ_{Max}). From simulated absorption spectra (Figure S3), we find that the maximum absorption wavelength (λ_{Max}) of the title compounds correspond to the first excited state $S_0 \rightarrow S_1$ in the ranges 290 to 366 nm and presented a large oscillator strength value (with the exception of E3, which exhibits a very weak oscillator strength (*f*=0.002))

The analyses of TD-DFT results display that the absorption spectra of the E-isomers are shifted to shorter wavelengths than those of Z-isomers (see Figure S3). This is in agreement with the existing experimental results and theoretical study at the ωB97XD/def2-SVPP level proposed by Mravec et al.[25]. Furthermore, the experimental $S_0 \rightarrow S_1$ transition energy of 1 and 7 isomers show red-shift energy absorption compared to TD-ωB97XD calculation by about 0.12 eV (for E1 and E7) and 0.55 eV (Z1 and Z7), see Table 5.

Table 5 Vertical transition energy ($\Delta E_{0\rightarrow1}$, eV) and wavelength ($\Delta\lambda_{0\rightarrow1}$, nm), oscillator strengths (f, dimensionless), charge transfer (q^{CT}, |e|), charge transfer distance (d^{CT}, Å) and dipole moment variation ($\Delta\mu$, D) associated to the $S_{0\rightarrow1}$ transition as calculated at the ωB97XD /6-311+g(d) in Ei and Zi compounds

	$E_{0\rightarrow1}$	$\lambda_{0\rightarrow1}$	f	d^{ct}	q^{ct}	$\Delta\mu$
E1	3.798(3.67)[a]	326	0.316	5.690	0.755	20.640
E2	3.780	327	0.315	5.884	0.767	21.671
E3	4.002	309	0.002	2.245	0.753	8.114
E4	3.931	315	0.463	4.771	0.666	15.252
E5	3.945	314	0.697	4.366	0.612	12.832
E6	3.844	322	0.923	2.335	0.674	7.557
E7	3.971(3.85)[a]	312	0.314	3.549	0.670	11.126
E8	3.556	348	0.56	3.659	0.663	10.590
E9	3.537	350	0.441	2.002	0.566	5.440
Z1	3.60(3.05)[a]	343	0.673	5.092	0.710	17.368
Z2	3.477	356	0.727	5.477	0.676	17.771
Z3	3.878	319	0.662	5.239	0.669	16.830
Z4	3.693	335	0.752	5.130	0.691	17.020
Z5	3.655	339	0.879	5.600	0.688	18.496
Z6	3.601	344	0.960	4.205	0.665	13.435
Z7	3.751(3.20)[a]	330	0.696	5.250	0.695	17.516
Z8	3.384	366	0.706	5.096	0.660	16.146
Z9	3.364	368	0.638	4.519	0.562	12.204
E10	3.962	312	0.615	4.256	0.672	13.736
E11	3.883	319	0.609	4.562	0.690	15.111
E12	4.370	283	0.635	3.651	0.601	10.543
E13	4.044	306	0.754	3.666	0.611	10.755
E14	3.998	310	0.934	3.368	0.566	9.165
E15	3.879	319	1.013	2.666	0.599	7.676
E16	4.092	302	0.690	3.749	0.589	10.600
E17	3.580	346	0.604	1.803	0.542	4.694
E18	3.540	350	0.430	3.120	0.509	7.629
Z10	3.642	340	0.659	3.551	0.608	10.370
Z11	3.519	352	0.704	4.509	0.649	14.044
Z12	3.925	315	0.627	3.078	0.561	8.291
Z13	3.718	333	0.743	3.242	0.587	9.146
Z14	3.6716	337	0.867	3.374	0.578	9.365
Z15	3.617	342	0.958	0.390	0.558	1.046
Z16	3.7940	326	0.6899	3.449	0.574	9.507
Z17	3.409	363	0.680	2.480	0.552	6.575
Z18	3.383	366	0.6262	0.740	0.502	1.783

[a]: experimental results from ref.25

For the E isomers (i=1-9), the wavelength of the first absorption transition is very close to that of the E–isomers (10 to 18, respectively). The same observation is found for Z isomers (i from 1 to 18), indicating that the introduction of NO_2 or CN group at R position has little effect on the absorption wavelength of E and Z isomers. Taking E6 and E15 as example, the $\lambda_{0\rightarrow1}$ is 322 and 315 nm, respectively and for Z6 and Z15 the $\lambda_{0\rightarrow1}$=343 nm for both (see Figure 4). On the other hand, the TD-DFT calculation on the title isomers reveals that the low-energy transitions $S_0 \rightarrow S_1$ is dominated by an electronic excitation from the HOMO to the LUMO and the shape of these two MOs depicts a significant charge transfer (CT) from the hydrazine part and ring 1 to ring 2 for the compounds 1, E2, 3, 4, Z5-Z10, E11, 12, 13, E14, Z15, 16, Z17 and Z18 and CT character from hydrazine part to ring1 for the isomers Z2, Z11 and Z14 (see Table S3 and Figures S1-S2) and intramolecular charge transfer (ICT) in the hydrazine part and ring1 for E5, E6, E8, E9, E15, E17 and E18 isomers. For the isomers 1-9 (substituted with NO_2 at the R position), the HOMO→LUMO+1 transition mainly results from Ar group to ring1, with the exception of the isomers E5, E6, E8, E9 and Z6 which exhibit an ICT character in the ring1 and Ar groups. On the other hand, for the isomers with CN unit at the R position, the HOMO→LUMO+1 transition can also be assigned as n,π→π* but from Ar group to ring2, with the exception for Z18 and E18 which exhibit an ICT character (see Table S3 and Figure S1).

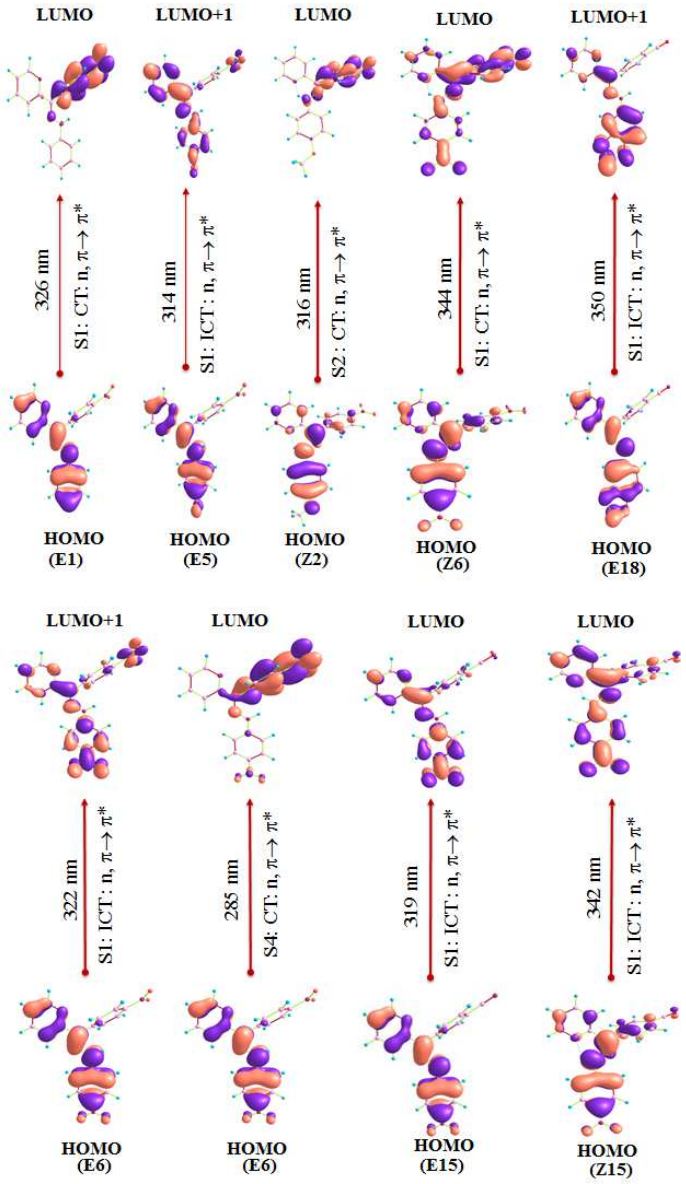

Figure 4. Molecular orbitals for S1, S2 and S4 absorption transitions

in the case of the Zi and Ei isomers (i = 1 to 9), it is clear that the transition HOMO → LUMO results in a more significant dipole moment (Δμ) compared to the transition HOMO → LUMO +1. Conversely, for the remaining compounds (10 to 18) substituted with a CN group at position R, the reverse pattern is observed (see Table S3). Taking Z2 and Z11 as example (see Figure 5), for Z2 the order of $\Delta\mu$ values follows as $\Delta\mu_{0\to2}$(H→L: 20.19) > $\Delta\mu_{0\to1}$(H→L +1: 17.77) and the reverse order is found for Z11 $\Delta\mu_{0\to2}$(H→L +1: 21.72) > $\Delta\mu_{0\to1}$(H→L : 14.04). In general, for the same transition HOMO → LUMO, LUMO+1, the $\Delta\mu$ values is larger in the 1-9 isomers than that in the corresponding 10-18 isomer, indicating that the presence of NO_2 group can enhance the $\Delta\mu$ and q^{CT} values more than the CN group. For example, Z2 (17.77D) is due to a transferred excitation charge $q^{CT} = 0.676$ |e| and an associated CT distance ($d^{CT} = 5.477$ Å) from HOMO to LUMO+1 (S0→S1) is larger than that of the excitation S0→S1 (from HOMO to LUMO) of Z11 ($q^{CT} = 0.649$ |e|, $d^{CT} = 4.509$Å and $\Delta\mu_{0\to1} = 14.04$ D). Generally, for the title photoswitches compounds we note that the Z-isomer undergoes a strong CT excitation with large CT distance (d^{CT}) and dipole moment variation (Δμ) compared to the E-isomers counterpart (compounds 1, 2 and 15 are exceptions to this, see Table S3). For instance, the $\Delta\mu_{0\to1}$, d^{CT} and q^{CT} of Z4 are calculated to be 17.02D, 5.13 Å and 0.691|e| larger than that the corresponding values of E4 (Figure5). Reversely, the Δμ, d^{CT} and q^{CT} of Z1and Z2 show small values with respect to that of E1 and E2 (Figure 5 and Table S3). It appears that the Z-isomer shape significantly increases the $\Delta\mu$, d^{CT} and q^{CT} values, this can be attributed to the electron delocalization effects in the ring N1-N2-C3-C4-N6…H (RAHB system).

Based on the quantum calculation, it can be observed that the strength of the hydrogen bond does not exert a significant effect on the optical properties of photoswitches (Table 5). Instead, the optical properties are influenced by conjugation, which is determined by the structure of the quasi-cycle (open or closed). It is crucial to emphasize that the opening or closing of the Resonance-Assisted Hydrogen Bond (RAHB) can significantly impact various molecular properties, including stability, acidity, basicity, reactivity, optical properties, and more.

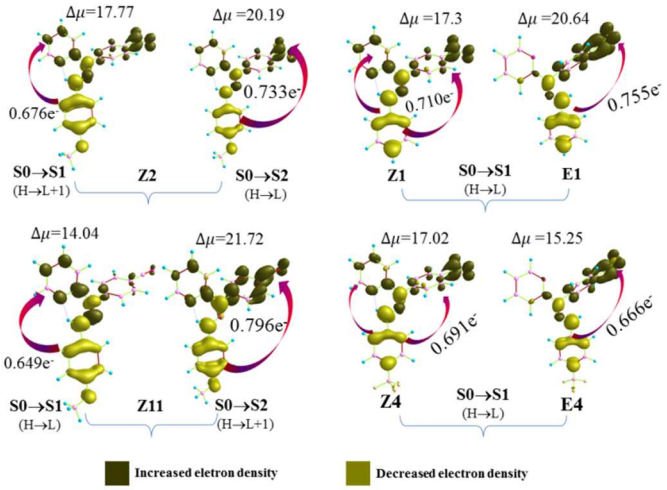

Figure 5. Electron density difference maps of Z1, E1, Z2, Z4, E4 and Z11 compounds from the ground state to the crucial excited state S0→S1 and S0→S2

Nonlinear optical properties

Dipole moment (μ, eV), isotropic polarizability (α), polarizability density (ρ a.u/Å³), nonlinear optical responses (NLO) e.g. first hyperpolarizability (β_0, a.u), second harmonic generation (β_{SHG}, a.u), electrooptic Pockels effect (β_{EOPE}, a.u), hyper-Rayleigh scattering (β_{HRS}, a.u) and depolarization ratio DR (static as well as dynamic) for all isomers are provided in Tables 6-7 and Tables S3, S4 and S5 (see Supporting Information).

Table 6 Static and dynamic isotropic average polarizability (α) and isotropic average polarizability volume (ρ) of Ei and Zi (i=1 to 18) compounds

	λ=∞		λ=695		λ=1064		λ=1340	
	α	ρ	α	ρ	α	ρ	α	ρ
E1	265	39	283	41	272	40	269	39
E2	284	42	302	44	291	43	289	42

E3	259	38	273	40	264	39	262	38
E4	280	41	297	44	287	42	284	42
E5	289	42	310	45	297	44	294	43
E6	291	43	313	46	300	44	296	43
E7	259	38	276	40	266	39	263	39
E8	313	46	336	49	322	47	319	47
E9	306	45	329	48	315	46	311	46
Z1	276	40	299	44	285	42	281	41
Z2	301	44	328	48	311	46	307	45
Z3	270	40	288	42	277	41	274	40
Z4	290	42	312	46	298	44	295	43
Z5	300	44	325	48	309	45	306	45
Z6	301	44	329	48	311	46	307	45
Z7	268	39	289	42	276	41	273	40
Z8	325	48	355	52	336	49	332	49
Z9	317	47	348	51	329	48	325	48
E10	265	39	282	41	272	40	270	40
E11	285	42	303	45	292	43	290	42
E12	259	38	270	40	264	39	262	38
E13	280	41	297	44	286	42	284	42
E14	290	43	310	45	298	44	295	43
E15	292	43	313	46	300	44	297	44
E16	260	38	276	40	266	39	264	39
E17	313	46	337	49	322	47	319	47
E18	306	45	329	48	315	46	312	46
Z10	275	40	297	44	284	42	281	41
Z11	299	44	325	48	309	45	306	45
Z12	269	39	286	42	276	40	273	40
Z13	288	42	310	45	297	44	294	43
Z14	300	44	325	48	310	45	306	45
Z15	301	44	328	48	312	46	308	45
Z16	268	39	288	42	276	40	273	40
Z17	324	48	353	52	335	49	331	49
Z18	317	47	346	51	328	48	324	48

Table 7 Calculated dipole moment (D, Debye), static hyperpolarizability ($\beta_0, \beta_{\mathrm{HRS}}^{\infty}$ a.u) and depolarization ratio (DR) calculated at ωB97XD /6-311+g(d) level forEi and Zi (i=1 to 18) compounds

	μ	β_0	$\beta_{HRS}^{\lambda=\infty}$	$DR^{\lambda=\infty}$		μ	β_0	$\beta_{HRS}^{\lambda=\infty}$	$DR^{\lambda=\infty}$
E1	5.098	1608	756	3.562	**Z1**	7.176	3906	1618	4.991
E2	5.340	2246	963	4.48	**Z2**	8.476	6498	2536	6.275
E3	4.980	1024	474	3.672	**Z3**	7.736	2965	1217	5.143
E4	5.035	1052	585	2.693	**Z4**	8.572	2980	1264	4.623
E5	6.282	312	546	1.584	**Z5**	9.924	2202	1055	3.428
E6	6.604	1928	1101	2.607	**Z6**	1.019	1530	1152	2.756
E7	7.080	995	553	2.695	**Z7**	5.343	2898	1261	4.294
E8	6.047	1446	730	3.114	**Z8**	7.510	3970	1674	4.711
E9	3.500	639	689	1.735	**Z9**	8.981	2570	1230	3.438
E10	4.905	1510	702	3.648	**Z10**	6.936	2632	1067	5.374
E11	5.261	2156	912	4.660	**Z11**	8.188	5017	1933	6.664
E12	4.870	845	387	3.765	**Z12**	7.649	1901	760	5.655
E13	4.992	987	529	2.829	**Z13**	8.516	1810	757	4.844
E14	6.293	683	548	1.959	**Z14**	9.853	1107	615	2.696
E15	6.626	2293	1164	3.085	**Z15**	1.020	1488	996	2.219
E16	6.895	936	497	2.871	**Z16**	5.114	1732	757	4.246
E17	5.888	1339	666	3,196	**Z17**	7.258	2390	1000	4.825
E18	3.398	1126	757	2.211	**Z18**	8.867	1160	646	2.689

The static and dynamic results for average linear polarizability <α> and dipole moment (μ) are presented in Table 6 and 7, respectively. The molecular polarizability is the ability of its electronic system to be distorted by an external field, according to our results in Table 6, the <α> value of the Z-isomer is slightly larger than the E-isomer counterpart. On the other hand, the most polarizable isomers are 8 and 17. These results show that the presence of the Ar8 group can enhance the polarizability value. The calculation shows that the polarizability density values (ρ) are similar and not sensitive to the type of Ar and R groups. Furthermore, we observed that the effect of the incident wavelength value (λ= 1340, 1064 and 695nm) on ⟨α⟩ and ⟨ ρ ⟩ is negligible.

As is well known the hyperpolarizability is sensitive to the several parameters such as the nature of the substituent (donor/ acceptor), the geometry of compounds, transition dipole moment, energy gap, electronic transition, incident wavelength (photon energy), etc. From Table S3 and Figure 6, one sees that the $\beta_{HRS}^{\lambda=\infty}$ and β_0 values of E-isomers substituted by either CN group or by NO_2 are very close, indicating that the replacement of NO_2 by CN group (at R position) has no effect on the static hyperpolarizability. Taking E8 and E17 as example, β_{HRS}^{∞}(E8) = 1.09 β_{HRS}^{∞}(E17). But in the case of Z-isomers, the introduction of NO_2 acceptor substituent at R position can increase the static hyperpolarizability (β_{HRS}^{∞} and β_0) about twice more than that of CN group, with the exception of Z6 and Z15 compounds for which their values are close (β_0(Z6) = 1.028 β_0 (Z15)), an effect which can be attributed to the small dipole moment (μ = 1.01 D). Furthermore, we can observe that the introduction of Ar_2 groups can increase the β_{HRS}^{∞} and β_0 compared with Ar_3 and Ar_5 groups (Figure 6 and Table 7). For example, the β_0 value of E2, Z2, E11 and Z11 is about 7, 4, 3 and 4 times larger than that of E5, Z5, E14 and Z14, respectively. The β_{HRS}^{∞} of Z2 (2536 a.u.) and Z11 (1933) are about 7 and 5 times greater than the values of E12 (Figure6).

Also, in this work, we studied the correlation between the energy gap (hardness) of Zi and Ei isomers and their hyperpolarizability in the static regime. The results show that $\beta_0[\beta_{HRS}^{\infty}]$ values increase with the decrease of the isomer energy gap. Taking Z2 as an example, the energy gap of Z2 is the smallest (6.304 eV) and its hyperpolarizability value is the largest (β_0= 6498 a.u.), which is in good agreement with the literature[74–77].

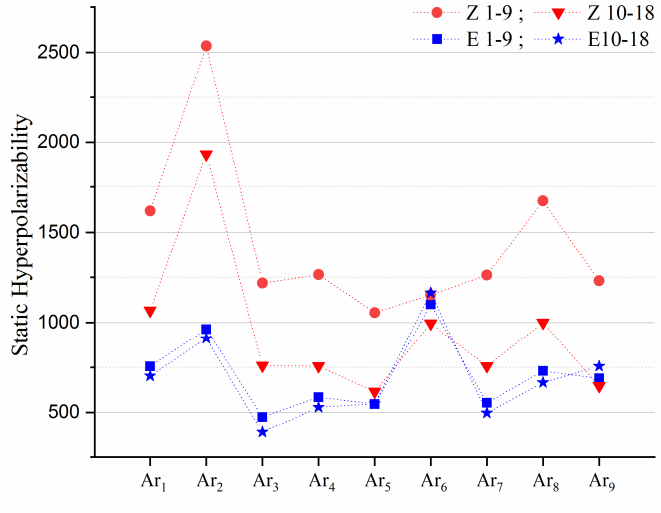

Figure 6 Variation of HRS hyperpolarizability in static regime of Z and E isomers

The magnitude of the hyperpolarizabilities of hydrazone photoswitches can be qualitatively rationalized using the two-state approximation, assuming that the S1 electronic excited state is the sole contributor to the sum-over-state expansion of the second-order nonlinear optical (NLO) response.[78,79]

$$\beta = \frac{3}{2}\frac{f_{0\to1} \times \Delta\mu_{0\to1}}{\Delta E_{0\to1}^{3}}$$

According to this formula β is directly linked to the transition dipole moment $\Delta\mu_{0\to1}$ and oscillator strength $f_{0\to1}$ and inversely linked to the third power of transition energy $\Delta E_{0\to1}$.

Based on our findings from Table 5 and Table S3 (Supplementary Information), it is evident that the Z isomer exhibits a lower excited energy ($\Delta E_{0\to1}$) and higher oscillator strength ($f_{0\to1}$) compared to its E-isomer counterpart. Our results clearly show that a decrease in the S0 → S1 transition energy and an increase in the value of $f_{0\to1}$ are directly associated with an increase in the hyperpolarizabilities of hydrazone photoswitches. Taking E1 and Z1 as example, E1 has a transition energy value of 3.798 eV, while Z1 has a lower value of 3.606 eV and the $f_{0\to1}$ value of Z1 is higher than that of E1. The DFT calculation shows that the Z1 exhibits a larger hyperpolarizability value compared to the E1 isomer. Similarly, we observed the same trend for the other isomers. Each isomer exhibits a lower transition energy ($\Delta E_{0\to1}$) and huge $f_{0\to1}$ value, generally displays larger hyperpolarizability, compared to its counterpart.

On the other hand, the larger hyperpolarizability values in the Z–isomers, compared to those in the E–isomers, can be due to the delocalization of electrons in the antiaromatic QCC (N1-N2-C3-C4-N6…H) in the Z–isomers, which does not exist in the E–isomers (Figure 1, Table 2 and S1). It means that destabilizing anti-aromatic behavior of quasi-cycle closed in the Z–isomers can reduce and grow the aromatic character in the ring 2 and 1, respectively, and this leads to enhance the hyperpolarizability values.

From our calculation, we observe that when the compound is in a Z form, the BLA decreases, which indicates a better electron delocalization and consequently the hyperpolarization increases. Figure 7 presents a nice linear relationship between BLA_{1-2} and static hyperpolarizability β_{HRS}^{∞} [β_0] of Z-isomers. It is important to note that, for the title isomers the variations of β_{HRS}^{∞} values are similar to those of β_0 values. Generally, the TD-DFT results indicated that the Z-isomers have low excitation energies of the first excited state and large transition dipole moments (Δμ), this being the necessary conditions to obtain high NLO response.

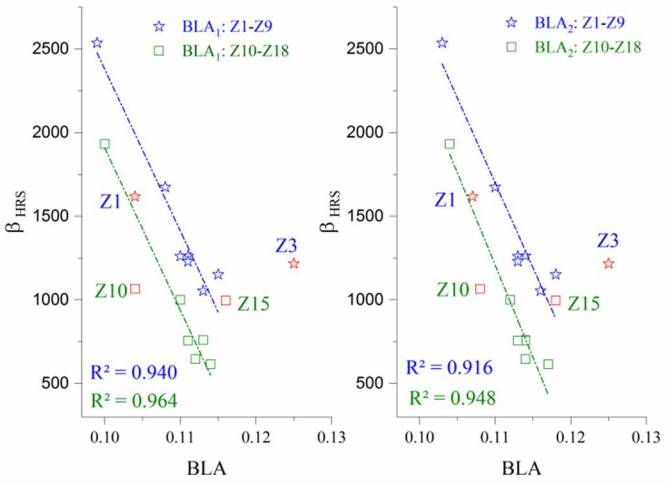

Figure 7 Correlation between BLA and static hyperpolarizability, the red points have been omitted from the correlation line

Mravec research group showed that increasing the EW character of the substituents on the Ar-ring leads to a little increase in the efficiency of the Z→E photoisomerization, whereas a large increase of quantum yield can be observed in the case of the back E→Z photoisomerization (in the order 3> 5 > 4> 7> 1> 6> 2; see Figure 8).[25] In general, our quantum calculation show inverse trend between photoisomerization quantum yields (Φ) and hyperpolarizability. Note, for instance the compound 2 (see Table 7 and Figure 6), this compound has the largest hyperpolarizability and the smallest photoisomerization QY (the EW substituents on the –C_6H_4 is OCH_3; Ar2=–C_6H_4-ρ- OCH_3). Furthermore, the trend photoisomerization QY is the same as for BLA values (see Table 1). On the other hand, we can attribute the small and large photoisomerization QY values ($\Phi_{Z\to E}$ <$\Phi_{E\to Z}$) to the hyperpolarizability of the first and second isomer of the mechanism. In other words, the Z→E photoisomerization mechanism[25] begins with the isomer having the largest hyperpolarizability (first isomer Z) and finishes with E-isomer (second isomer) that has a small hyperpolarizability and this mechanism displays a weak $\Phi_{Z\to E}$ value. In the same context, the E→Z photoisomerization starts with the E-isomers (first isomer) having the smaller hyperpolarizability than the second isomer Z, and present a larger $\Phi_{E\to Z}$ value than the $\Phi_{Z\to E}$ (see Table 7-8 and Figure 8). Taking the compound 3 as an example, the photoisomerization quantum yields of $\Phi_{E3\to Z3}$ is larger than that of $\Phi_{Z3\to E3}$ (Φ= 12.3 and 0.8, respectively)[25] and the

hyperpolarizability value of Z3 is larger than that of E3 ($\beta[Z3] \approx 3\beta[E3]$), see Table 8.

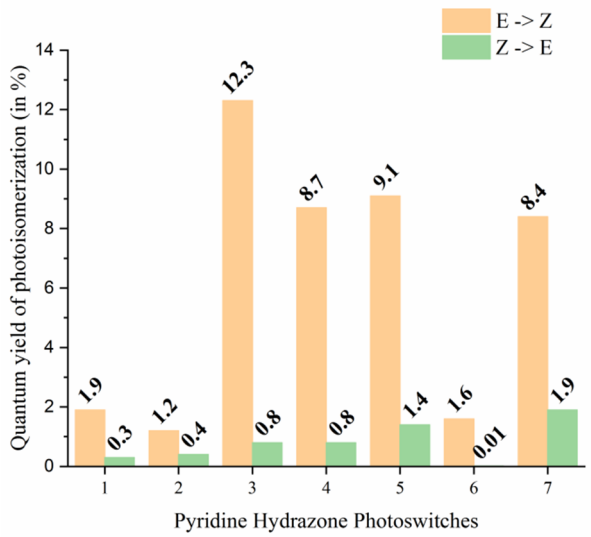

Figure 8 Evolution of photoisomerization quantum yields (Φ) with the increasing EW character of the hydrazine ring (the values from the reference [25])

From our study we can conclude that there is a proportional relationship between photoisomerization quantum yield and hyperpolarizability of the second isomer and there is an inversely proportional relationship between Φ and β of first isomer. These relationships will be the object of further investigations.

Table 8 The Static and dynamic hyperpolarizability $\beta^{\lambda}_{Zi}/\beta^{\lambda}_{Ei}$ ration (where $\eta^{\lambda} = \beta^{\lambda}_{Zi}/\beta^{\lambda}_{Ei}$; η^{∞}_{HRS}, η_0 and η^{∞}_{SHG}) to the Z- and E- isomers

Zi/Ei	η^{∞}_{HRS}	η^{695}_{HRS}	η^{1064}_{HRS}	η^{1307}_{HRS}	η_0	η^{695}_{SHG}	η^{1064}_{SHG}	η^{1307}_{SHG}
1	2.140	14.097	2.385	2.267	2.429	13.464	2.541	2.465
2	2.633	6.485	3.131	2.883	2.893	5.854	3.312	5.713
3	2.567	5.578	2.980	2.780	2.895	5.597	3.224	3.051
4	2.160	6.191	2.4656	2.328	2.832	6.107	2.809	2.766
5	1.932	10.947	2.7012	2.357	7.057	11.286	5.252	5.943
6	1.046	6.083	1.034	1.037	0.793	4.287	0.733	0.754
7	2.280	4.939	2.555	2.434	2.912	4.863	2.854	2.837
8	2.293	0.221	2.792	2.556	2.745	0.184	3.059	2.893
9	1.785	0.212	2.191	2.012	4.021	0.076	4.732	4.496
10	1.519	7.919	1.739	1.636	1.743	7.936	1.915	1.829
11	2.119	11.437	2.442	2.280	2.326	11.102	2.593	2.450
12	1.963	4.078	2.237	2.108	2.249	4.275	2.492	2.366
13	1.431	4.866	1.705	1.577	1.833	4.982	2.001	1.908
14	1.122	8.439	1.667	1.391	1.620	9.172	2.681	2.304
15	0.855	2.092	0.7881	0.817	0.648	0.753	0.550	0.592
16	1.523	3.438	1.727	1.634	1.850	3.553	1.968	1.906
17	1.501	0.169	1.767	1.631	1.784	0.151	2.001	1.880
18	0.853	0.078	0.941	0.901	1.030	0.059	1.276	1.192

According to the TD-DFT results ($\lambda_{Max} \equiv \lambda_{0\to1}$) we calculated the hyperpolarizability ($\beta^{\lambda}_{HRS}, \beta^{\lambda}_{SHG}$ *and* β^{λ}_{EOPE}) of the studied isomers at a near resonant wavelength of 695 nm (≈ 2×λ_{Max}) and a nonresonant wavelength of 1064 nm and 1340 nm. Our results at the dynamic regime presents an excellent linear relationship between hyper-Rayleigh scattering (β^{λ}_{HRS}) and second harmonic generation (β^{λ}_{SHG}), see Figure 9.

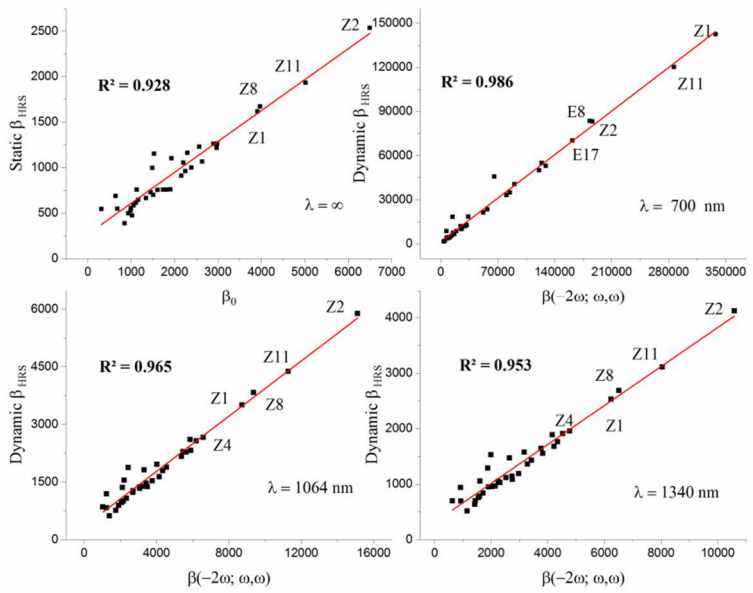

Figure 9 Correlation between $\beta^{\infty}_{HRS} \leftrightarrow \beta_0$ and $\beta^{\lambda}_{HRS} \leftrightarrow \beta^{\lambda}_{SHG}$

As can be seen in Figure 10, that the hyperpolarizability value increases with decreasing wavelength of the incident light, i.e. β(695) > β(1064) > β(1340) > β(∞). Obviously, the β^{λ}_{SHG} and β^{λ}_{HRS} values dramatically increase at the 695 nm wavelength more than at λ= 1340 nm and 1064 nm, this can be attributed to the larger resonance or dispersion at 290-366 nm according to the TD-DFT results (Table S3). As examples, Z1 exhibits the largest response at λ = 695 nm $\beta^{695}_{HRS}[\beta^{695}_{SHG}] = 142500\,[337600]$a.u.), while this isomer possess small values at λ = ∞, 1340, 1064 nm. By way of explanation, the hyperpolarizability $\beta^{\lambda}_{HRS}[\beta^{\lambda}_{SHG}]$ of Z1 at 695 nm is approximately 39 and 55 times higher than at 1340, 1064 nm, respectively. On the other hand, the magnitude of β(-ω; ω, 0) is slightly enhanced with increasing frequency of the incident light compared with β^{λ}_{HRS} and β^{λ}_{SHG} (Table S4). Taking Z2 and E5 as examples, the β^{695}_{EOPE} value of Z2 (12100 a.u.) is evaluated to be the largest and E5 possess a small value of β^{695}_{EOPE} (771 a.u.) which is almost two times larger than that of the β^{λ}_{EOPE} at 1340 and 1064 nm.

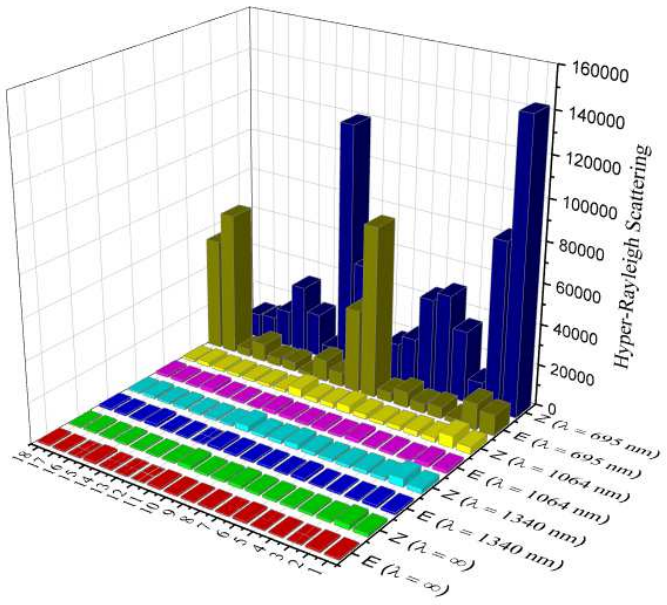

Figure 10 Calculated first hyperpolarizabilities of Z and E isomers, in the zero frequency limit and frequency-dependent fields

In most cases in static and dynamic regime (λ= ∞, 1064 and 1307 nm), the hyperpolarizability $\beta_0, \beta_{SHG}^{\lambda}, \beta_{HRS}^{\lambda}$ of Z-isomers are in the range of 2−7 times as large as those of the corresponding E-isomer. For example, the β_0 value of Z5 is 2200 a.u., which is 7 times larger than that of the corresponding E5. With the exception of compounds 6, 15 and 18, where the values of Z are smaller than that of E, for instance, $\beta_{SHG}^{\lambda}\ (Z15) \approx 1/2\ \beta_{SHG}^{\lambda}\ (E15)$ see Table 8. On the other hand, the β_{SHG}^{695} $[\beta_{HRS}^{695}]$ of Z-isomers is 2-14 times larger than that of the corresponding E-isomers. With the exception of compounds 8, 9, 17 and 18, where E8, E9, E17 and E18 have the largest β_{SHG}^{695} $[\beta_{HRS}^{695}]$ value which is about 5, 13, 7 and 17 [5, 5, 6 and 13] times as large as those of Z-isomers Z8, Z9, Z17 and Z18, respectively (Table 8).

In addition, dynamic perturbations were introduced to explore the effect of frequency dispersion. To provide a comparison, we utilized two fundamental optical wavelengths λ= 1340 and 1064 nm (used in NLO measurements) along with 695 nm (derived from TD-DFT results). This allowed us to assess the contribution of dispersion correction to the NLO response in these isomers. To quantify this correction, we used the frequency dispersion factor between static and dynamic at a definite wavelength is depicted by the ratio $\beta_{\mathrm{HRS}}^{\lambda}/\beta_{\mathrm{HRS}}^{\infty}$, and is listed in Table S6. We can observe that the dispersion of optical nonlinearity at λ = 695 nm of E8, E17, Z1, E18, Z11, E9, Z14, Z10, Z5, Z6 and Z2, respectively have maximum frequency dispersion factor (from 115 to 32) which can be attributed to the TD-DFT results, where $\lambda_{Max} = \sim\frac{1}{2}\ 695\ nm$. In contrast to the isomers E3 and E12 (λ_{Max}=309 and 283 nm, respectively) display the smallest dispersion factor (about 4.36) and the other isomers show a moderate values (from 6 to 29) at λ = 695 nm. As can be seen, the frequency dispersion factor at incident laser (λ= 1340 and 1064 nm) of the title compounds is in the range 1-5.

Our findings indicate that the frequency dispersion factor is greater at higher frequencies compared to lower frequencies; the weak frequency of incident light should be chosen to count the 2nd NLO coefficients in the experiment[80]. Regarding possible applications, in terms of writing and reading stored information on photochromic materials, the non-resonant character of NLO enables reading outside the absorption band, in this case, erasure during reading can be avoided[19]. Clearly, the larger hyperpolarizability does emerge when the incident wavelength of dispersion is equal or closer to twice the wavelength in the first transition ($\lambda_{0\to1}$).

To further explore the origin of the first hyperpolarizability of the title compounds (E and Z isomers) the polarization scan of HRS intensity $I_{\Psi V}^{2\omega}$ has also been calculated, and the relationship between the $I_{\Psi V}^{2\omega}$ and polarization angle Ψ is plotted (see Figure S5 and plotted for the compounds 1 and 5 in Figure 11) the $\beta_{\mathrm{J=1}}$ and $\beta_{\mathrm{J=3}}$ are listed in Table S5.

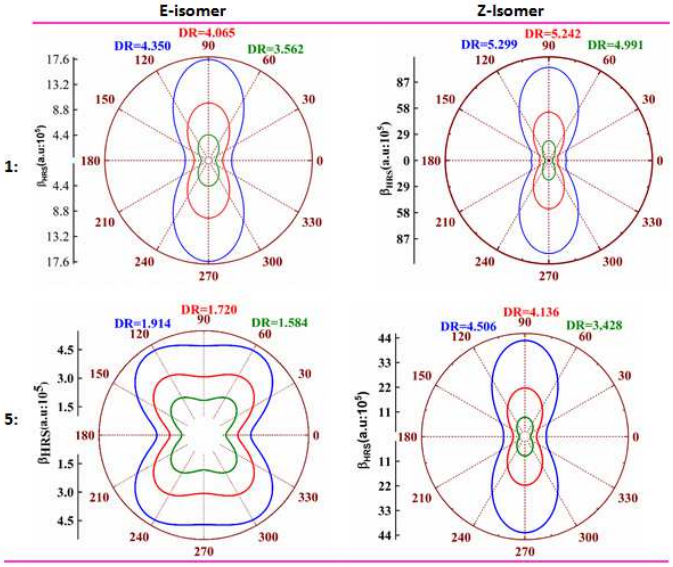

Figure 11. Relationship between $I_{\Psi V}^{2w}$ and polarization angle Ψ of Z and E isomers (green static, red λ=1340 nm, blue λ=1064 nm

From Figure 12, we can conclude that the DR values are sensitive to the nature of the Ar and R substituents, the geometry of isomers (Z and E shapes) as well as the wavelength of the incident light. We observed that, at λ= ∞, 1064 and 1307nm the DR value decreases in the following order: DR(λ=1064) >DR(λ=1340) >DR (λ= ∞) also, from this Figure, it seems that the Z-isomer exhibit larger DR than the corresponding E-isomer. In contrast at 695nm, the depolarization ratio of E-isomer is larger than that of Z-isomer counterpart, which can be attributed to its resonance or dispersion at λ_{Max}.

On the other hand, at λ= ∞, 1064 and 1307 nm, it can be found that E4, E13, E6, Z6, E15, Z15, E7, E16, E8, E17, E9, E18 and Z18 molecules are considered as octupolar molecules with large octupolar contributions ($\beta_{\mathrm{J=3}} > \beta_{\mathrm{J=1}}$), while E1, E10, Z10, E2, Z2, E11, Z11, E3, Z3, E12, Z12, Z4, Z13, Z5, Z7, Z16, Z8, Z17, Z9 molecules are considered as dipolar molecules and dipolar contributions $\beta_{\mathrm{J=1}}$ larger than the $\beta_{\mathrm{J=3}}$ (see Table S5 and Figure S5). For the Z1 and E5, illustrated in Figure 11, the DR amounts to 4.991 and 1.584, respectively, a value close to 5 and 1.5; these values are characterizing ideal dipolar and typical octupolar systems, respectively.

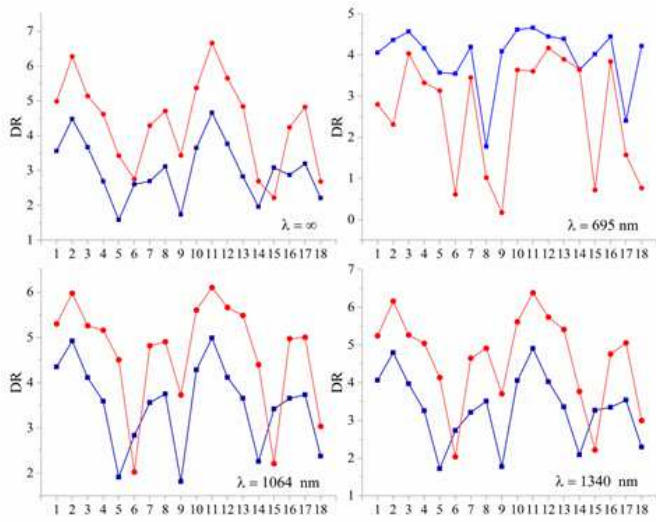

Figure 12 Evolution of the depolarization ratio (DR) in static and dynamic regime (red: Z-isomer, blue: E-isomer)

The quantum chemical calculation shows that the Z-isomers exhibit the largest response, whereas the corresponding E-isomers exhibit smaller values at static and dynamic regimes. It is worth noting that the larger NLO responses are strongly related to the hydrogen bond, the electron-withdrawing character of the substituents on the Ar hydrazine moiety and on the ring 2 and photoisomerization quantum yields $\Phi_{E\rightarrow Z}$. Among the 18 E/Z isomers theoretically studied, Z2 is the most promising for future applications in the NLO field.

Conclusions

Systematic DFT and TD-DFT calculations have been carried out on extended series of substitutional derivatives of pyridine photoswitches. The structural, reactivity parameters, linear and nonlinear optical properties of all compounds differing by a CN and NO_2 substitution on the ketone fragment at the position R and Ar ring in the hydrazine fragment have been analysed in detail.

The quantum calculation indicates that the Z-isomers are proposed to be a promising candidate for the 2nd –order nonlinear optical applications due to its lower excited energy, smaller BLA values, weaker energy gap, larger dipole moment variations in the first excited state, smaller electron localization in the antiaromatic ring (QCC), and higher photoisomerization quantum yields $\Phi_{E\rightarrow Z}$ than that of the corresponding E-isomers. To the best of our knowledge, this work evidences that the delocalization strength enhanced by the resonance-assisted hydrogen bond can improve the second order NLO responses of the hydrazone photoswitches, especially due to the delocalized electrons in the antiaromatic ring (QCC) in Z-isomers.

Regarding the NLO properties, DFT calculation indicates that the CN and NO_2 groups have the same effect on the static hyperpolarizability of E-isomers. For Z-isomers, the introduction of NO_2 at R position increases the β_{HRS}^{∞} and β_0 about twice more than that of CN group. Furthermore, their introduction into the Ar2 group increases the hyperpolarizability (β_{HRS}^{∞} and β_0) compared with Ar3 and Ar5 groups.

Regarding the nonlinear optical properties of isomers, we found that the frequency-dependent hyperpolarizability (λ = 695 nm) of title isomers are larger than the static regime revealing an eminent hyperpolarization, due to the delocalized electrons in isomers. By increasing the incident wavelengths from λ = 695 nm to λ=1064 and 1307 nm, the dispersion of optical nonlinearity of isomers shows a smaller value than at λ = 695 nm. Our results indicates that the resonance effect of the hyperpolarizability is amplified with the decrease of incident wavelength (λ = 695). A good correlation is obtained between $\beta_{HRS}^{\infty} \leftrightarrow \beta_0$ and $\beta_{HRS}^{\lambda} \leftrightarrow \beta_{SHG}^{\lambda}$ as well as between BLA and static hyperpolarizability.

Author Contributions

All the authors discussed the results.

Conceptualization and methodology: D.H and H.C; Investigation: D.H, N.K, M.Z, D.Y, S.L, C.M and H.C; Writing – Original Draft Preparation: D.H and H.C; Writing – Review & Editing: D.H, N.K, M.Z, D.Y, S.L; C.M and H.C.; Data Curation: D.H, N.K, M.Z, D.Y, S.L, C.M and H.C. All authors have read and agreed to the published version of the manuscript.

Conflicts of interest

There are no conflicts to declare.

ORCID

Meriem ZAIDI: 0000-0002-7358-1999

Douniazed HANNACHI: 0000-0001-6664-179X

Christophe MORELL: 0000-0002-6321-8723

Salima LAKEHAL: 0000-0003-1265-3597

Henry CHERMETTE: 0000-0002-5890-7479

Acknowledgements

The authors gratefully acknowledge the GENCI/ CINES for HPC resources/computer time (Project cpt2130), and the PSMN of the ENS-Lyon for computing resources.

Notes and references

1 K. Matsuda and M. Irie, *J. Am. Chem. Soc.*, 2000, **122**, 7195–7201.

2 C. G. Liu, Z.-M. Su, X.-H. Guan and S. Muhammad, *Mol. Phys.*, 2011, **115**, 23946–23954.

3 M. N. Chaur, D. Collado and J. M. Lehn, *Chem. - A Eur. J.*, 2011, **17**, 248–258.

4 M. Schulze, M. Utecht, A. Hebert, K. Ru, P. Saalfrank and P. Tegeder, *J. Phys. Chem. Lett.*, 2015, **6**, 505–509.

5 L. Greb and J. Lehn, *J. Am. Chem. Soc. Irradiat.*, 2014, **136**, 13114−13117.

6 M. Zaidi, D. Hannachi and H. Chermette, *Inorg. Chem.*, 2021, **60**, 6616–6632.
7 D. Kamli, D. Hannachi and H. Chermette, *New J. Chem.,* 2023, **47**, 1234–1246.
8 M. S. Kodikara, R. Stranger and M. G. Humphrey, *Coord. Chem. Rev.*, 2018, **375**, 389–409.
9 Y. Y. Liang, B. Li, X. Xu, F. Long Gu and C. Zhu, *J. Comput. Chem.*, 2019, **40**, 971–979.
10 N. Baggi, E. Garoni, A. Colombo, C. Dragonetti, S. Righetto, D. Roberto, J. Boixel, V. Guerchais and S. Fantacci, *Polyhedron*, 2018, **140**, 74–77.
11 C. Andraud, F. Cyril, B. Olivier, H. Chermette and P. L. Baldeck, *Adv. Polym. Sci.*, 2008, **214**, 149–203.
12 M. Schulze, M. Utecht, T. Moldt, D. Przyrembel, C. Gahl, M. Weinelt and P. Tegeder, *Phys.Chem.Chem.Phys.,* 2015, **17**, 18079–18086.
13 A. Goulet-hanssens and C. J. Barrett, *J. Polym. Sci. PART A Polym. Chem.*, 2013, **51**, 3058–3070.
14 D. J. Van Dijken, P. Kovar, S. P. Ihrig and S. Hecht, *J. Am. Chem. Soc.*, 2015, **137**, 14982–14991.
15 K. J. Chen, A. D. Laurent and D. Jacquemin, *J. Phys. Chem. C*, 2014, **118**, 4334–4345.
16 P. Zhao, D. Wang, H. Gao, J. Zhang, Y. Xing, Z. Yang, H. Cao and W. He, *Dye. Pigment.*, 2018, **162**, 451–458.
17 A. J. Garza, O. I. Osman, N. A. Wazzan, S. B. Khan, G. E. Scuseria and A. M. Asiri, *Comput. Theor. Chem.*, 2013, **1022**, 82–85.
18 T. Woller, P. Geerlings, F. De Proft, B. Champagne and M. Alonso, *J. Phys. Chem. C*, 2019, **123**, 7318–7335.
19 J. A.Delaire, E. Ishow and K. Nakatani, *Photoreact. Org. Thin Film.*, 2002, 305–329.
20 L. Yan, T. Zhang and Z. Su, *J. Phys. Chem. A POMs.29−31*, 2013, **117**, 10783−10789.
21 S. Ishihara, J. P. Hill, A. Shundo, G. J. Richards, J. Labuta, K. Ohkubo, S. Fukuzumi, A. Sato, M. R. J. Elsegood, S. J. Teat and K. Ariga, *J. Am. Chem. Soc.*, 2011, **133**, 16119–16126.
22 B. He and O. S. Wenger, *J. Am. Chem. Soc.*, 2011, **133**, 17027–17036.
23 Y. Zhang, H. Wang, J. Ye, X. Li and Y. Qiu, *Organomet. Chem.*, 2019, **888**, 29–36.
24 M. Samoc, N. Gauthier, M. P. Cifuentes, F. Paul, C. Lapinte and M. G. Humphrey, *Angew. Chemie*, 2006, **118**, 7536–7539.
25 B. Mravec, Š. Budzák, M. Medved', L. F. Pašteka, C. Slavov, T. Saßmannshausen, J. Wachtveitl, J. Kožíšek, L. Hegedüsová, J. Filo and M. Cigáň, *J. Org. Chem.*, 2021, **86**, 11633–11646.
26 B. Mravec, J. Filo, K. Csicsai, V. Garaj, M. Kemka, A. Marini, M. Mantero, A. Bianco and M. Cigáň, *Phys. Chem. Chem. Phys.*, 2019, **21**, 24749–24757.
27 B. Mravec, A. Marini, M. Tommasini, J. Filo, M. Cigáň, M. Mantero, S. Tosi, M. Canepa and A. Bianco, *ChemPhysChem*, 2021, **22**, 533–541.
28 M. N. Chaur, D. Collado and J. M. Lehn, *Chem. A Eur. J.*, 2011, **17**, 248–258.
29 J. Da Chai and M. Head-Gordon, *Phys. Chem. Chem. Phys.*, 2008, **10**, 6615–6620.
30 J. Da Chai and M. Head-Gordon, *J. Chem. Phys.*, 2008, **128**, 084106–14.
31 G. A. Petersson and A.-L. Mohammad A, *J. Chem. Phys.*, 1991, **9**, 6081–6090.
32 G. A. Petersson, A. Bennett, T. G. Tensfeldt, M. A. Al-Laham, W. A. Shirley and J. Mantzaris, *J. Chem. Phys.*, 1988, **89**, 2193–2218.
33 S. Grimme, *J. Comput. Chem.*, 2006, **27**, 1787–1799.
34 M. J. Frisch, E. Al. and G. 09, *Revision B.01, Gaussian, Inc.: Wallingford CT,* .
35 R. A. Kendall, T. H. Dunning and R. J. Harrison, *J. Chem. Phys.*, 1992, **96**, 6796–6806.
36 C. Lee, W. Yang and R. G. Parr, *Phys. Rev. B*, 1988, **37**, 785–789.
37 H. Chermette, *J. Comput. Chem.*, 1999, **20**, 129–154.
38 R. G. Parr, L. V. Szentpály and S. Liu, *J. Am. Chem. Soc.*, 1999, **121**, 1922–1924.
39 T. Le Bahers, C. Adamo and I. Ciofini, *J. Chem. Theory Comput.*, 2011, **7**, 2498–2506.
40 T. Lu and F. Chen, *J. Comput. Chem.*, 2012, **33**, 580–592.
41 M. Kamiya, H. Sekino, T. Tsuneda, K. Hirao and M. Kamiya, *J. Chem. Phys.*, 2005, **122**, 234111.
42 J. E. Rice, R. D. Amos, S. M. Colwell, N. C. Handy and J. Sanz, *J. Chem. Phys.*, 1990, **93**, 8828–8839.
43 R. Bersohn, P. A. O. Yoh-Han and H. L. Frisch, *J. Chem. Phys.*, 1966, **45**, 3184–3198.
44 A. Plaquet, M. Guillaume, B. Champagne, F. Castet, L. Ducasse, J. L. Pozzo and V. Rodriguez, *Phys. Chem. Chem. Phys.*, 2008, **10**, 6223–6232.
45 F. Castet, E. Bogdan, A. Plaquet, L. Ducasse, B. Champagne and V. Rodriguez, *J. Chem. Phys.*, 2012, **136**, 24506–15.
46 H. Louis, I. B. Onyebuenyi, J. O. Odey, A. T. Igbalagh, M. T. Mbonu, E. A. Eno, A. M. S. Pembere and E. O, 2021, **11**, 28433–28446.
47 P. S. V. Kumar, V. Raghavendra and V. Subramanian, *J. Chem. Sci.*, 2016, **128**, 1527–1536.
48 D. Paul, J. Deb and U. Sarkar, *ChemistrySelect*, 2020, **5**, 6987–6999.
49 E. Espinosa, I. Alkorta, J. Elguero and E. Molins, *J. Chem. Phys.*, 2002, **117**, 5529.
50 C. F. G. E. J.Baerends, T.Ziegler, A. J.Atkins, J.Autschbach, D.Bashford, A.Bérces, F. M.Bickelhaupt, C.Bo, P. M.Boerrigter, L.Cavallo, D. P.Chong, D. V.Chulhai, L.Deng, R. M.Dickson, J. M.Dieterich, D. E.Ellis, M.van Faassen, L.Fan, T. H.Fischer, *ADF2016.01, SCM, Theor. Chem. Vrije Univ. Amsterdam, Netherlands, 2016, http//www.scm.com.*
51 G. Te Velde, F. M. Bickelhaupt, E. J. Baerends, C. Fonseca Guerra, S. J. A. Van Gisbergen, J. G. Snijders and T. Ziegler, *J. Comput. Chem.*, 2001, **22**, 931–967.
52 M. Palusiak and T. M. Krygowski, *Chem. - A Eur. J.*, 2007, **13**, 7996–8006.
53 E. Arunan, G. R. Desiraju, R. A. Klein, J. Sadlej, S. Scheiner, I. Alkorta, D. C. Clary, R. H. Crabtree, J. J. Dannenber, P. Hobza, H. G. Kjaergaard, A. C. Legon, B. Mennucci and D. J. Nesbitt, *Pure Appl. Chem.*, 2011, **83**, 1637–1641.
54 P. von R. Schleyer, C. Maerker, A. Dransfeld, H. Jiao, N. J. R. V. E. Hommes, D.- Erlangen and R. V February, *Am. Chem.*

Soc., 1996, **118**, 6317–6318.
55 P. von R. Schleyer, B. Kiran, D. V. Simion and T. S. Sorensen, *J. Am. Chem. Soc.*, 2000, **122**, 510–513.
56 D. Hannachi, N. E. H. Amrane, L. Merzoud and H. Chermette, *New J. Chem.*, 2021, **45**, 13451–13462.
57 J. Li and A. Y. Rogachev, *Phys. Chem. Chem. Phys.*, 2016, 11781–11791.
58 A. Ayadi, L. Mydlova, N. Zouari, M. Makowska-janusik, B. Sahraoui and A. El-ghayoury, *Opt. Mater. (Amst).*, 2016, 1–9.
59 R. N. Butler and S. M. Johnston, *J. Chem. Soc. Perkin Trans. 1*, 1984, 2109–2116.
60 M. A. Al-Sheikh and M. H. Elnagdi, *Molecules*, 2009, **14**, 4406–4413.
61 S. M. Landge and I. Aprahamian, *J. Am. Chem. Soc.*, 2009, **131**, 18269–18271.
62 X. Su and I. Aprahamian, *Org. Lett.*, 2011, **13**, 30–33.
63 S. M. Landge, E. Tkatchouk, D. Benítez, D. A. Lanfranchi, M. Elhabiri, W. A. Goddard and I. Aprahamian, *J. Am. Chem. Soc.*, 2011, **133**, 9812–9823.
64 X. Su, M. Lõkov, A. Kütt, I. Leito and I. Aprahamian, *Chem. Commun.*, 2012, **48**, 10490–10492.
65 C. Lu, B. Htan, S. Fu, C. Ma and Q. Gan, *Tetrahedron*, 2019, **75**, 4010–4016.
66 P. Gilli, V. Bertolasi, L. Pretto, V. Ferretti and G. Gilli, *J. Am. Chem. Soc.*, 2004, **126**, 3845–3855.
67 V. Bertolasi, P. Gilli, V. Ferretti and G. Gilli, *J. Am. Chem. Soc.*, 1991, **113**, 4917–4925.
68 G. Gilli, F. Bellucci, V. Ferretti and V. Bertolasi, *J. Am. Chem. Soc.*, 1989, **111**, 1023–1028.
69 E. Espinosa, E. Molins and C. Lecomte, *Chem. Phys. Lett.*, 1998, **285**, 170–173.
70 I. Mata, I. Alkorta, E. Espinosa and E. Molins, *Chem. Phys. Lett.*, 2011, **507**, 185–189.
71 L. J. Karas, P. R. Batista, R. V. Viesser, C. F. Tormena, R. Rittner and P. R. De Oliveira, *Phys. Chem. Chem. Phys.*, 2017, **19**, 16904–16913.
72 A. V. Afonin, A. V. Vashchenko and M. V. Sigalov, *Org. Biomol. Chem.*, 2016, **14**, 11199–11211.
73 L. R. Domingo, M. J. Aurell, P. Pérez and R. Contreras, *Tetrahedron*, 2002, **58**, 4417–4423.
74 L. Wang, J. Ye, H. Wang, H. Xie and Y. Qiu, *Sci. Rep.*, 2017, **7**, 1–11.
75 K. S. Thanthiriwatte and K. M. Nalin de Silva, *J. Mol. Struct. THEOCHEM*, 2002, **617**, 169–175.
76 R. V. Solomon, P. Veerapandian, S. A. Vedha and P. Venuvanalingam, *J. Phys. Chem. A*, 2012, **116**, 4667–4677.
77 N. Hou, R. Feng and X.-H. Fang, *Int. J. Quantum Chem.*, 2022, **122**, 1–14.
78 J. L. Oudar and D. S. Chemla, *J. Chem. Phys.*, 1976, **66**, 2664–2668.
79 C. Tonnelé and F. Castet, *Photochem. Photobiol. Sci.*, 2019, **18**, 2759–2765.
80 M. Zhang, C. Wang, W. Wang, N. Ma, S. Sun and Y. Qiu, *J. Phys. Chem. A*, 2013, **117**, 12497–12510.